HHS Public Access

Author manuscript

Neuroimage. Author manuscript; available in PMC 2016 November 15.

Published in final edited form as:

Neuroimage. 2015 November 15; 122: 281–287. doi:10.1016/j.neuroimage.2015.07.073.

Dynamics of Respiratory and Cardiac CSF Motion Revealed with Real-time Simultaneous Multi-Slice EPI Velocity Phase Contrast Imaging

Liyong Chen[*], **Alexander Beckett**[*], **Ajay Verma**, and **David A. Feinberg**

[1]University of California, Berkeley

[2]Advanced MRI Technologies, Sebastopol, CA

[3]Biogen-Idec, Boston MA

Abstract

Cerebrospinal fluid (CSF) dynamics have been mostly studied with cardiac-gated phase contrast MRI combining signal from many cardiac cycles to create cine-phase sampling of one time averaged cardiac cycle. The relative effects of cardiac and respiratory changes on CSF movement are not well understood. There is possible respiration driven movement of CSF in ventricles, cisterns, and subarachnoid spaces which has not been characterized with velocity measurements. To date, commonly used cine-phase contrast techniques of velocity imaging inherently cannot detect respiratory velocity changes since cardiac gated data acquired over several minutes randomizes respiratory phase contributions. We have developed an extremely fast, real-time and quantitative MRI technique to image CSF velocity in simultaneous multi-slice (SMS) echo planar imaging (EPI) acquisitions of 3 or 6 slice levels simultaneously over 30 seconds and observe 3D spatial distributions of CSF velocity. Measurements were made in 10 subjects utilizing a respiratory belt to record respiratory phases and visual cues to instruct subjects on breathing rates. A protocol is able to measure velocity within regions of brain and basal cisterns covered with 24 axial slices in 4 minutes, repeated for 3 velocity directions. These measurements were performed throughout the whole brain, rather than in selected line regions so that a global view of CSF dynamics could be visualized. Observations of cardiac and breathing-driven CSF dynamics show bidirectional respiratory motion occurs primarily along the central axis through the basal cisterns and intraventricular passageways and to a lesser extent in the peripheral Sylvian fissure with little CSF motion present in subarachnoid spaces. During inspiration phase, there is upward (inferior to superior direction) CSF movement into the cranial cavity and into the lateral ventricles and a reversed direction in expiration phase.

Corresponding Author: David A. Feinberg, PhD, MD, Helen Wills Neuroscience Institute, University of California, Berkeley, Berkeley, CA, Advanced MRI Technologies, Sebastopol, CA, David.feinberg@advancedmri.com.

[*]authors made equal contribution

Keywords

EPI; velocity; CSF; simultaneous multi-slice; multiband; phase contrast; respiratory; cardiac

Introduction

Cerebrospinal fluid (CSF) velocity is a complex phenomenon and is known to be driven by vascular pulsations (Feinberg and Mark, 1987). Although respiration is known to influence CSF movement (Klose et al., 2000c; Schroth and Klose, 1992), it is also known that breathing related susceptibility changes can influence the signal phase (Raj et al., 2001b; Raj et al., 2000b) in echo planar imaging (EPI) in fMRI. In general, MR signal magnitude changes seen with CSF motion have been found to be inherently non-quantitative, and cannot show the direction of CSF motion (Bergstrand et al., 1985; Bradley et al., 1986). Spin labeling techniques have shown CSF displacement with breathing and valsalva maneuvers (Yamada et al., 2013; Bhadelia et al., 2013). To date, respiratory driven CSF velocity has not been directly measured and consequently the relative effects of cardiac and respiratory changes on CSF motion are not well understood. More specifically, the directions and phases of respiration driven movement of CSF in distinct compartments of ventricles, cisterns, and cortical subarachnoid spaces are not known. Better understanding of these velocity distributions in time and space are likely occurring through links between cardiothoracic physiology, cerebrovascular and intracranial CSF dynamics.

Earlier techniques of measuring velocity with phase imaging (Feinberg and Mark, 1987; Enzmann and Pelc, 1992; Moran, 1982) inherently could not detect respiratory changes since data over several minutes was sorted or regrouped by its time in the cardiac cycle; hence each image has randomized respiratory phase contributions. Real-time EPI does not require the sorting and grouping of data as images can be acquired in less than 100 ms. Earlier techniques of velocity phase in spin echo EPI were cardiac gated to study cardiac driven brain motion (Poncelet et al., 1992) and by not being real-time acquisitions they did not reveal respiratory changes in velocity. Conventional EPI time series data have shown signal intensity variations in aqueductal CSF synchronous with respiration (Klose et al., 2000c; Schroth and Klose, 1992), however these sequences could not show the direction of CSF motion nor quantify velocity as the work presented here.

Utilizing a recent development of Simultaneous Multi-slice (SMS) snapshot echo planar imaging (EPI) (Larkman et al., 2001; Feinberg et al., 2010; Moeller et al., 2010; Setsompop et al., 2012; Feinberg and Setsompop, 2013), time series data at different levels in the brain can be obtained simultaneously without compromising temporal resolution. We have developed SMS EPI with velocity encoding to create an extremely fast and quantitative MRI technique to image CSF movement throughout the intraventricular passageways and subarachnoid spaces for real-time CSF imaging (Feinberg et al., 2012; Chen et al., 2014; Beckett et al., 2015). Given CSF velocity can be measured in real time without gating or reordering, we extended the length of the time series to half a minute in order to detect potential changes occurring over several respiratory cycles that would not be readily apparent over a single respiratory cycle. This takes advantage of simultaneous time series

data by avoiding errors from normal variations occurring over time and has enabled studies of normal physiological breathing on CSF movement within the brain and subarachnoid spaces. Large regions of the brain and its surrounding CSF spaces were scanned to study CSF dynamics in normal subjects under different breathing conditions.

Methods

A pulse sequence for velocity phase imaging utilizing simultaneous multi-slice (SMS) EPI was developed as shown in Figure 1. This adaptation of the SMS EPI sequence with additional velocity encoding (VENC) bipolar gradient pulses. VENC is defined as the velocity range corresponding to phase shifts spanning from −180° to +180°. VENC≥2.5cm/s allowed real-time continuous imaging of multiple slices simultaneously at about 80ms sampling rate. In early experiments, a dual-band saturation pulse is applied for outer volume suppression for zoomed imaging increasing resolution without aliasing artifact. In the experiments with repeated measures in 10 subjects, full field of view imaging was used. Studies were performed on a Siemen 3T Trio Scanner with 32-channel receiver coil and all subjects gave written informed consent following institutional guidelines.

The other parameters are as below: repetition time (TR)=78–82ms, echo time (TE)=30–32ms; in-plane under-sampling factor=2; partial Fourier factor=6/8; spatial resolution=1.5×1.5mm^2; slice thickness=3–5mm; matrix size=128×128; 24 slices; number of simultaneous slices excited by multiband pulse (MB)=3 or 6; 1/3 field-of-view (FOV) shift in controlled aliasing. The velocity phase shifts were encoded with bipolar gradient pulse (VENC=2.5~5cm/s, noteworthy: each bipolar is set to be ±5~±10 cm/s due to the alternative velocity encoding) using phase subtraction sliding between TRs in which the bipolar pulse had alternating polarity. An algorithm with kernel size of 3 was used to separate the images, as previously described (Setsompop et al., 2012). The 30 seconds real-time scan was performed for each multiband time-series acquisition of one velocity direction. CSF movement in multiple directions was measured by repeating the 30-second scans with different bipolar gradient pulses. A complete 4D (24 slices) velocity imaging of brain and CSF is acquired in acquisition time = 30s×8 sets×3 velocity directions = 12 minutes.

The single-slice EPI phase contrast imaging without SMS technique was compared at the same acquisition parameter except the slice number. Also, conventional cardiac-gated GRE phase contrast imaging technique was scanned on the aqueduct CSF area for comparison with following parameters: in-plane resolution=1.5×1.5mm^2, slice thickness=5mm, VENC=10 cm/s, TR=16.35 ms, TE=5.8 ms, acquisition time = 1.7 minutes.

For all the SMS EPI phase contrast experiments, a respiratory sensor band at the level of the diaphragm was used to track the diaphragm motion during CSF scan. The subjects were guided to breathe in five different patterns (‘free’, ‘fast’, ‘slow’, ‘breath-hold’ after inspiration and ‘breath-hold’ after expiration). The subjects performed these different breathing rates by observing a visual periodic pattern displayed on a screen within the scanner. Ten healthy subjects were scanned in total, and one was removed due to substantial motion. All subjects were scanned for the 24 slice protocol, and 6 of those subjects were

also scanned with a 3 slice protocol at different speeds. In addition, 5 of the subjects were scanned for the comparison of the real-time EPI and cardiac-gated GRE sequences.

Data Analysis

Subtraction of pairs of phase images acquired time sequentially in adjacent TRs generated the time series of phase contrast images for velocity measurements. These phase difference maps (phase contrast images) were corrected for phase offsets errors in the data (e.g. those introduced by eddy currents)Walker et al. (1993): the phase difference images of static tissue region were used to calculate linearly varying phase offset errors in three spatial directions, and these linearly fitted phase offset were then subtracted from the each phase difference image.

Regions of interest (ROIs) for data analysis were identified based on a combination of the magnitude images from the velocity encoded scans, and series of T2 weighted images collected at the beginning of the scan. A series of ROIs in the CSF passages in the central axis of the brain were identified, as well as ROIs in the subarachnoid space.

The phase difference time series from regions of interest (ROI) were multiplied by VENC/π to generate velocity curves. For better presentation, the velocity time series were low-pass filtered at the expected respiratory ((10^{th} order Butterworth filter, <0.5hz). The low-passed timeseries were compared to the diaphragm motion as measured by the respiratory sensor band.

To assess the respiratory and cardiac modulations in the timeseries, a power analysis was performed and amplitudes were summed in two frequency bands, a “respiratory” frequency band (f<0.5 Hz) and a “cardiac” frequency band (0.65 < f < 1.65 Hz).

To validate whether the CSF velocities using the SMS sequence matched those from a single slice acquisitions, the low-passed time series from an ROI in the aqueduct from a single slice acquisition was compared to two time series from multi-slice acquisitions in the same ROI, with a similar and differing cued breathing frequency.

Results

Figure 2 shows the magnitude and phase difference images from a single SMS acquisition compared with the equivalent phase difference image from a standard single slice acquisition. The two timeseries from an ROI placed in the aqueduct during an identical breathing scheme are also shown, showing good agreement between the two methods. Correlations were significantly higher between single- and multi-slice scans with same breathing scheme (two sample t-test, $p< 0.01$) than two multi-slice scans with different breathing schemes using the data from 4 subjects. Four subjects were also scanned with a standard cardiac gated GRE sequence, and the resulting velocity curves were compared with the timeseries from the same ROI in the real-time EPI scan, while subjects were instructed to minimize their breathing to isolate the cardiac component of the velocity modulations. Although a quantitative comparison of the two methods was not performed, side-by-side comparison of the velocity curves from the two methods showed a comparable range of

velocities, indicating that the methods were in good general agreement (Figure 2 (Bottom) and Supplemental Figure 1). A full quantitative comparison of the cardiac gated versus the real-time methods is beyond the scope of the current paper, owing to the differences in temporal resolution and acquisition method.

The aqueduct CSF velocity curves of through-plane velocity encoding direction from different breathing schemes are shown in Figure 3 (Data from an additional subject is shown in Supplemental Figure 2). The modulations of CSF flow are shown at different breathing rates, both freely and cued by an external stimulus; while cessation of breathing lessens or removes these modulations. These modulations were in addition to the changes in velocity due to cardiac modulation, which were shown with and without breathing by the subject. The low frequency modulation (defined as < 0.5 Hz) well matched the frequency of respiration as measured by a belt while the subject was being scanned. Note the rise from the trough of the belt curve marks the transition to inspiration, which is shown below the zero velocity line.

SMS techniques allow acquisition of multiple slices simultaneously, so as to obtain CSF velocity from multiple planes. Figure 4 shows timeseries data from 3 ROIs in 3 different slices from one subject breathing at two different speeds: fast breathing (~0.17 Hz) and slow breathing (~0.125 Hz). The changes in CSF velocity match up well with breathing and the frequency of modulation matching that of the respiration belt. This pattern is repeated across ROIs from all 3 slices, although the velocities in the upper slice are much lower.

To increase the number of slices that can be acquired, the multiband factor can be increased to 6, as shown in Figure 5. The timeseries plotted from ROIs across the 6 slices all show both cardiac and respiratory type modulations, with the modulations matching up across slices and amplitudes appearing to drop off at the highest slices.

To examine the effects of respiration across the whole brain, subjects were scanned during slow breathing. 24 axial slices with 3 velocity encoding directions from 9 subjects were acquired and 11 CSF ROIs were selected, as shown in Figure 6. The minimum and maximum velocities varied across the different ROIs (Figure 6A), being generally higher in the superior-inferior (SI) direction which is through-plane in these axial studies and anterior-posterior (AP) directions, dropping off at the highest levels measured, and being lower in ROIs placed in the sulci. After low-pass filtering to preserve low frequency changes, respiration-like modulations (Figure 6B) were generally lower than in the raw data, also being higher in the FH and AP directions. Low frequency modulations are seen in the SI and AP directions in a number of ROIs (Figure 6C), with amplitudes dropping off in more dorsal areas. Amplitudes in the cardiac range (~1.1 Hz, Figure 6D) also show the majority of power in the SI and AP directions, also dropping off in the most dorsal regions. The respiratory and cardiac frequencies calculated from different ROIs and subjects (Figure 6) were consistent to each other and agreed well with literature. Greater variation in the ‘cardiac’ frequencies is present due to the variation in heart rate between subjects, whereas respiration was cued and kept constant.

To test the relationship between breathing phase (inspiration/expiration) and CSF flow velocity, we calculated the mean velocity in the Foramen Magnum (FM) and Aqueduct (Aq) during the cued inspiration period (dots expanding in visual stimulus) and the cued expiration period (dots contracting). In the 3 slice acquisitions comparing different breathing rates, we found positive mean velocities during inspiration and negative mean velocities during expiration periods across all 6 subjects. In the faster breathing condition at the FM (0.4071/−0.1131 cm/s) and Aq (0.4013/−0.1356 cm/s) the difference between the two periods was significant (two sample t-tests, p = 0.002/0.0013). This pattern of results repeated in the slow breathing condition (FM: 0.3328/−0.0735 cm/s, p=0.002; AQ: 0.2133/−0.505, p=0.0204). Shifting the windows by 1/4 of a respiration cycle (1.5s for fast breathing, 2s for slow breathing), so that the windows contained a mixture of both cued inspiration and expiration, removed this effect. This was also found in the 24 slice acquisition protocol across all 9 subjects, with positive velocities during inspiration and negative during expiration periods in the FM (0.1218/−0.1407 cm/s) and Aq (0.1/−0.11 cm/s), with significant differences between the two periods (p=0.0007/0.0208).

Discussion

In this work, SMS EPI phase contrast imaging was used to measure respiratory and cardiac modulated CSF velocity in a number of ROIs simultaneously. The respiratory modulation of CSF velocity was discovered by collecting data under different breathing conditions, in addition to the well-known cardiac modulations (Figures 3–5). The frequency of modulations seen in the CSF velocity timeseries from a selection of ROIs primarily matched up with the frequency’s of two physiological sources: respiration and cardiac pulsation. The similarity in frequency between the CSF velocity modulation and the cued breathing speed strongly suggests that respiration has an effect on CSF flow velocities, both direction and speed.

During two different breathing rates, the findings held that the upward directed CSF velocity occurred in the inspiration phase, while downward directed velocity occurred in the expiration phase, as confirmed by statistical comparison of CSF velocities during the two phases. Drawing exact conclusions about the coupling mechanism between inspiration/expiration and changes in CSF velocity direction is not however currently possible. Variations in subjects breathing responses to the stimulus, possible delays between subject's breathing and a change in the belt recording as would occur with diaphragmatic movement rather than chest movement, and other unknown physiological factors make it difficult to determine the exact onset of changes in CSF direction with respect to breathing.

To our knowledge, this is the first reporting of CSF velocities in the cranium driven by breathing obtained with non-invasive measurement. Prior work observed non-specific signal intensity changes in EPI time series (Kao et al., 2008; Klose et al., 2000c; Schroth and Klose, 1992) and susceptibility changes (Raj et al., 2001a; Raj et al., 2000a) but not velocity phase changes. These previous studies detected respiratory oscillation frequencies but did not identify the direction of CSF motion, nor its direction with respect to the respiratory phase, nor could they quantify magnitudes of CSF velocity differing in different areas of the brain and subarachnoid spaces as could our study that provided high sensitivity to small

velocity by using larger bipolar pulses. Signal tagging (Yamada et al., 2013) has been used to detect CSF displacement in selected line regions occurring during breath hold, however it does not measure velocity nor view extensive regions in multiple 2D images simultaneously as in the current study. Our non-invasive MRI velocity study finds negligible CSF movement in the sulci and subarachnoid spaces at the outer surface of the brain under normal conditions.

Besides the respiratory and cardiac modulation, additional modulations at low frequencies were also seen (Fig 3, Supplemental Figure 2). Potential sources for these modulations could be low frequency variations in respiration (as evidenced by similar low frequency modulations appearing in the respiratory belt data) or a separate source of low frequency variations in CSF flow velocity, for example the B-Waves seen in EPI data (Friese et al., 2004; Klose et al., 2000a). Future scans with a longer total acquisition time would be able to investigate these potential very-low frequency modulations directly. The low frequency modulations at respiratory frequencies were absent when subjects performed breath holding (Fig 3), although there is some suggestion that there may be a global drop in velocity for breath holding after both expiration and inspiration. Potential causes of this, including changes in intracranial pressure due to increased blood volume, or some other physiological origin, are unclear from the data collected and will be investigated further in future work.

There are both spatial and temporal factors in image encoding that generally effect quantitation of CSF velocities by phase contrast imaging (Barkhof et al., 1994; Kolbitsch et al., 1999; Sharma et al., 2008), with some factors specific to real-time imaging. Velocity phase aliasing can occur in higher-velocity areas such as the aqueduct and in this respect, our whole-head protocol used a low VENC to maximize sensitivity to respiratory changes in velocity which increased the possibility of aliasing. Partial volume effects in lower spatial resolution (mixing signal from stationary tissue in with the signal from CSF), and averaging voxels with variable velocities across the ROIs themselves can both reduce measured velocity. The temporal resolution in real-time phase contrast imaging can affect measured phase differences, more prone to occur with faster cardiac modulation than with slower respiratory modulation.

Another factor is the chosen direction of the velocity encoding, where for example the orientation of through-plane velocity can be chosen parallel to the aqueduct or alternatively as in these experiments a set of 3 directions of velocity are acquired in all locations to completely measure velocity components. As mentioned earlier, conventional cine reordered or cardiac gated phase contrast techniques cannot capture respiratory velocity changes, whereas the presented real-time phase contrast reproducibly quantify bidirectional CSF velocities correlated with respiratory modulation.

For possible medical applications, real-time phase contrast velocity imaging could be applied to evaluate respiration velocity effects in Chiari syndrome which results in a narrower CSF passageway through the foramen magnum, raising CSF velocities or possibly obstructing respiratory CSF movement through the base of the skull. In other applications, these techniques might be useful for studying physiological, and factors affecting intrathecal drug delivery to the brain, where the different breathing rates and resulting CSF velocity

may directly effect drug transport through the foramen magnum to the brain. As such, this may also influence the distribution of biomarkers and intrathecally-dosed drugs along the neuroaxis (Linninger et al., 2008).

In conclusion, we have measured velocity of CSF during the breathing cycle in the basal cisterns, foramen Magendie, fourth ventricle, aqueduct and foramen Monroe. CSF motion at lower velocity was observed in the Sylvian fissure with little respiratory and cardiac motion present in smaller sulci in subarachnoid spaces. To our knowledge these results are the first real-time continuous velocity imaging of CSF. This has been facilitated by the simultaneous multi-slice technique that inherently has several times greater data acquisition efficiency than single slice techniques. In these physiological studies, the simultaneity of velocity recordings at different slice levels also eliminates variability from heart rate changes that could otherwise occur. Although previous work has shown oscillations in CSF signal intensity during breathing, we have shown the direction and magnitude of CSF motion during inspiration and expiration. Using real-time SMS-EPI phase contrast imaging, CSF dynamics were visualized and quantified in normal physiology and these results differed from prior theories of CSF motion, which did not attribute such large CSF volume shifts to respiration.

Supplementary Material

Refer to Web version on PubMed Central for supplementary material.

References

Barkhof F, Kouwenhoven M, Scheltens P, Sprenger M, Algra P, Valk J. Phase-contrast cine MR imaging of normal aqueductal CSF flow. Effect of aging and relation to CSF void on modulus MR. Acta Radiol. 1994; 35:123–130. [PubMed: 8172735]

Beckett, A.; Chen, L.; Verma, A.; Feinberg, D. ISMRM 23rd Annual Meeting. ISMRM; 2015. Velocity phase imaging with simultaneous multi-slice EPI reveals respiration driven motion in spinal CSF.

Bergstrand G, Bergstrom M, Nordell B, Stahlberg F, Ericsson A, Hemmingsson A, Sperber G, Thuomas KA, Jung B. Cardiac gated MR imaging of cerebrospinal fluid flow. J Comput Assist Tomogr. 1985; 9:1003–1006. [PubMed: 2932480]

Bhadelia R, Madan N, Zhao Y, Wagshul M, Heilman C, Butler J, Patz S. Physiology-based MR imaging assessment of CSF flow at the foramen magnum with a Valsalva maneuver. American Journal of Neuroradiology. 2013; 34:1857–1862. [PubMed: 23620074]

Bradley WG Jr, Kortman KE, Burgoyne B. Flowing cerebrospinal fluid in normal and hydrocephalic states: appearance on MR images. Radiology. 1986; 159:611–616. [PubMed: 3704142]

Chen, L.; Beckett, A.; Verma, A.; Feinberg, D. ISMRM 22nd Annual Meeting. ISMRM; 2014. 7D velocity phase imaging with zoomed simultaneous multi-slice EPI reveals respiration driven motion in brain and CSF; p. 1489

Enzmann DR, Pelc NJ. Brain motion: measurement with phase-contrast MR imaging. Radiology. 1992; 185:653–660. [PubMed: 1438741]

Feinberg, D.; Chen, L.; Vu, AT. ISMRM 20th Annual Meeting. ISMRM; 2012. Multiband Velocity EPI; p. 2499

Feinberg DA, Mark AS. Human brain motion and cerebrospinal fluid circulation demonstrated with MR velocity imaging. Radiology. 1987; 163:793–799. [PubMed: 3575734]

Feinberg DA, Moeller S, Smith SM, Auerbach E, Ramanna S, Gunther M, Glasser MF, Miller KL, Ugurbil K, Yacoub E. Multiplexed echo planar imaging for sub-second whole brain FMRI and fast diffusion imaging. PLoS One. 2010; 5:e15710. [PubMed: 21187930]

Feinberg DA, Setsompop K. Ultra-fast MRI of the human brain with simultaneous multi-slice imaging. J Magn Reson. 2013; 229:90–100. [PubMed: 23473893]

Friese S, Hamhaber U, Erb M, Klose U. B-waves in cerebral and spinal cerebrospinal fluid pulsation measurement by magnetic resonance imaging. Journal of computer assisted tomography. 2004; 28:255–262. [PubMed: 15091131]

Kao YH, Guo WY, Liou AJ, Hsiao YH, Chou CC. The respiratory modulation of intracranial cerebrospinal fluid pulsation observed on dynamic echo planar images. Magn Reson Imaging. 2008; 26:198–205. [PubMed: 17826939]

Klose U, Strik C, Kiefer C, Grodd W. Detection of a relation between respiration and CSF pulsation with an echoplanar technique. Journal of Magnetic Resonance Imaging. 2000a; 11:438–444. [PubMed: 10767073]

Klose U, Strik C, Kiefer C, Grodd W. Detection of a relation between respiration and CSF pulsation with an echoplanar technique. J Magn Reson Imaging. 2000c; 11:438–444. [PubMed: 10767073]

Kolbitsch C, Schocke M, Lorenz IH, Kremser C, Zschiegner F, Pfeiffer KP, Felber S, Aichner F, Hormann C, Benzer A. Phase-contrast MRI measurement of systolic cerebrospinal fluid peak velocity (CSFV(peak)) in the aqueduct of Sylvius: a noninvasive tool for measurement of cerebral capacity. Anesthesiology. 1999; 90:1546–1550. [PubMed: 10360850]

Larkman DJ, Hajnal JV, Herlihy AH, Coutts GA, Young IR, Ehnholm G. Use of multicoil arrays for separation of signal from multiple slices simultaneously excited. J Magn Reson Imaging. 2001; 13:313–317. [PubMed: 11169840]

Linninger AA, Somayaji MR, Erickson T, Guo X, Penn RD. Computational methods for predicting drug transport in anisotropic and heterogeneous brain tissue. J Biomech. 2008; 41:2176–2187. [PubMed: 18550067]

Moeller S, Yacoub E, Olman CA, Auerbach E, Strupp J, Harel N, Ugurbil K. Multiband multislice GE-EPI at 7 tesla, with 16-fold acceleration using partial parallel imaging with application to high spatial and temporal whole-brain fMRI. Magn Reson Med. 2010; 63:1144–1153. [PubMed: 20432285]

Moran PR. A flow velocity zeugmatographic interlace for NMR imaging in humans. Magn Reson Imaging. 1982; 1:197–203. [PubMed: 6927206]

Poncelet BP, Wedeen VJ, Weisskoff RM, Cohen MS. Brain parenchyma motion: measurement with cine echo-planar MR imaging. Radiology. 1992; 185:645–651. [PubMed: 1438740]

Raj D, Anderson AW, Gore JC. Respiratory effects in human functional magnetic resonance imaging due to bulk susceptibility changes. Physics in medicine and biology. 2001a; 46:3331. [PubMed: 11768509]

Raj D, Anderson AW, Gore JC. Respiratory effects in human functional magnetic resonance imaging due to bulk susceptibility changes. Phys Med Biol. 2001b; 46:3331–3340. [PubMed: 11768509]

Raj D, Paley DP, Anderson AW, Kennan RP, Gore JC. A model for susceptibility artefacts from respiration in functional echo-planar magnetic resonance imaging. Physics in medicine and biology. 2000a; 45:3809. [PubMed: 11131201]

Raj D, Paley DP, Anderson AW, Kennan RP, Gore JC. A model for susceptibility artefacts from respiration in functional echo-planar magnetic resonance imaging. Phys Med Biol. 2000b; 45:3809–3820. [PubMed: 11131201]

Schroth G, Klose U. Cerebrospinal fluid flow. II. Physiology of respiration-related pulsations. Neuroradiology. 1992; 35:10–15. [PubMed: 1289732]

Setsompop K, Gagoski BA, Polimeni JR, Witzel T, Wedeen VJ, Wald LL. Blipped-controlled aliasing in parallel imaging for simultaneous multislice echo planar imaging with reduced g-factor penalty. Magn Reson Med. 2012; 67:1210–1224. [PubMed: 21858868]

Sharma AK, Gaikwad S, Gupta V, Garg A, Mishra NK. Measurement of peak CSF flow velocity at cerebral aqueduct, before and after lumbar CSF drainage, by use of phase-contrast MRI: utility in the management of idiopathic normal pressure hydrocephalus. Clin Neurol Neurosurg. 2008; 110:363–368. [PubMed: 18282655]

Walker PG, Cranney GB, Scheidegger MB, Waseleski G, Pohost GM, Yoganathan AP. Semiautomated method for noise reduction and background phase error correction in MR phase velocity data. Journal of Magnetic Resonance Imaging. 1993; 3:521–530. [PubMed: 8324312]

Yamada S, Miyazaki M, Yamashita Y, Ouyang C, Yui M, Nakahashi M, Shimizu S, Aoki I, Morohoshi Y, McComb JG. Influence of respiration on cerebrospinal fluid movement using magnetic resonance spin labeling. Fluids Barriers CNS. 2013; 10:36. [PubMed: 24373186]

Highlights

- Real-time imaging of cardiac and respiratory components of CSF velocity.
- Simultaneous multi-slice (SMS) phase contrast (PC) EPI.
- Respiratory CSF velocity for first time seen in direction and magnitude
- Inspiration phase CSF directed superiorly into ventricles and foramen magnum
- Reversed in expiration phase giving bidirectional respiratory motion.

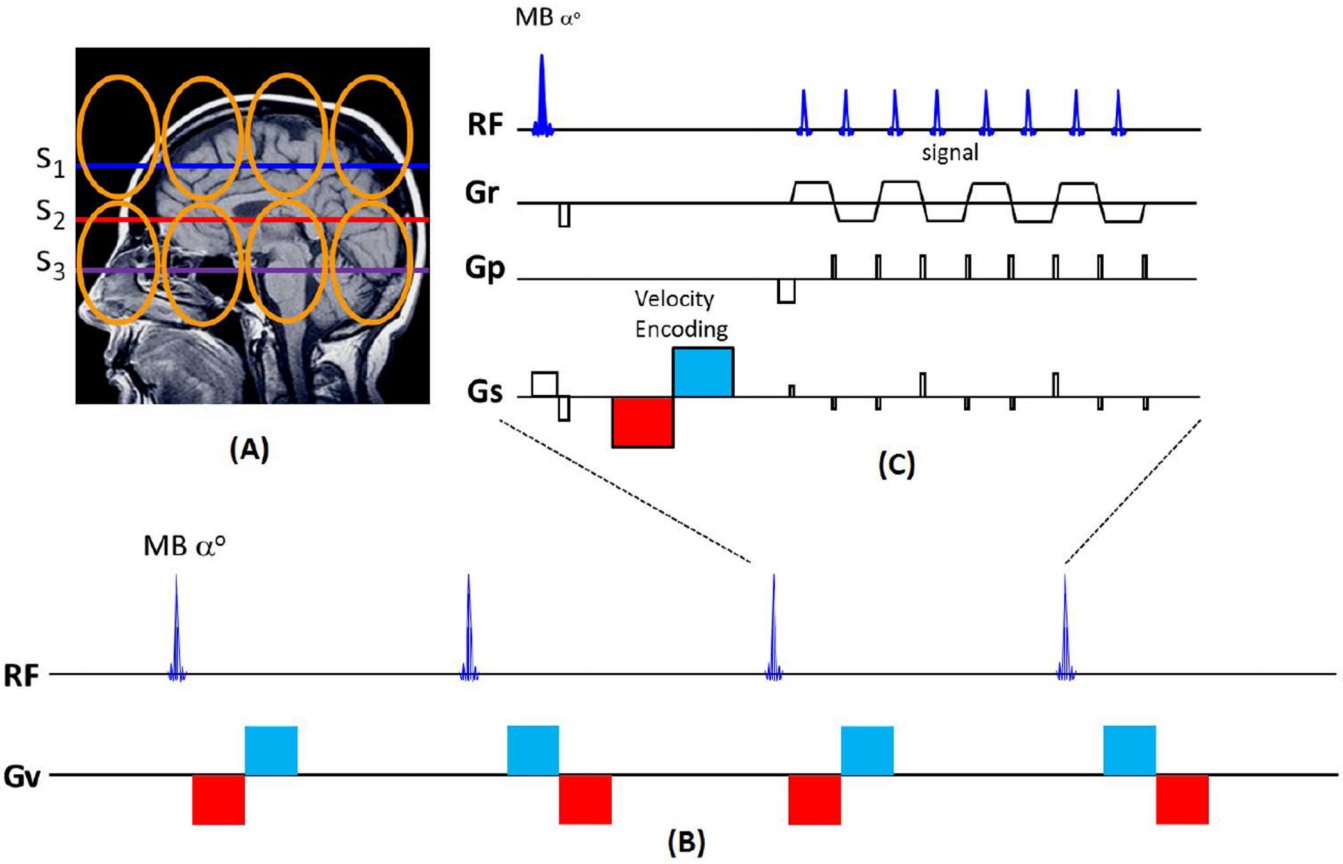

Figure 1.

Diagram of simultaneous multi-slice (SMS)-EPI velocity pulse sequence. (A) Three simultaneous excitation planes (S^1-S^3). Coil array coverage (orange loops) is shown. (B) The pulse sequence acquisition scheme illustration for multiband velocity imaging. The polarity of the velocity phase encoding +/− is determined by the polarity of the bipolar pulse (red/blue vs. blue/red) used in each TR of the encoding scheme. Sequential pairs of time frames encoded with alternating phase polarity are subtracted to create each velocity image. The time series of velocity images can generate the velocity movie. (C) The SMS-EPI velocity pulse sequence diagram. The multiband (MB) excitation pulse is followed by the (velocity encoding) bipolar gradient (red/blue) pulse and the SMS-EPI readout. Radiofrequency (RF), read gradient (Gr), phase encoding gradient (Gp), slice selective gradient (Gs).

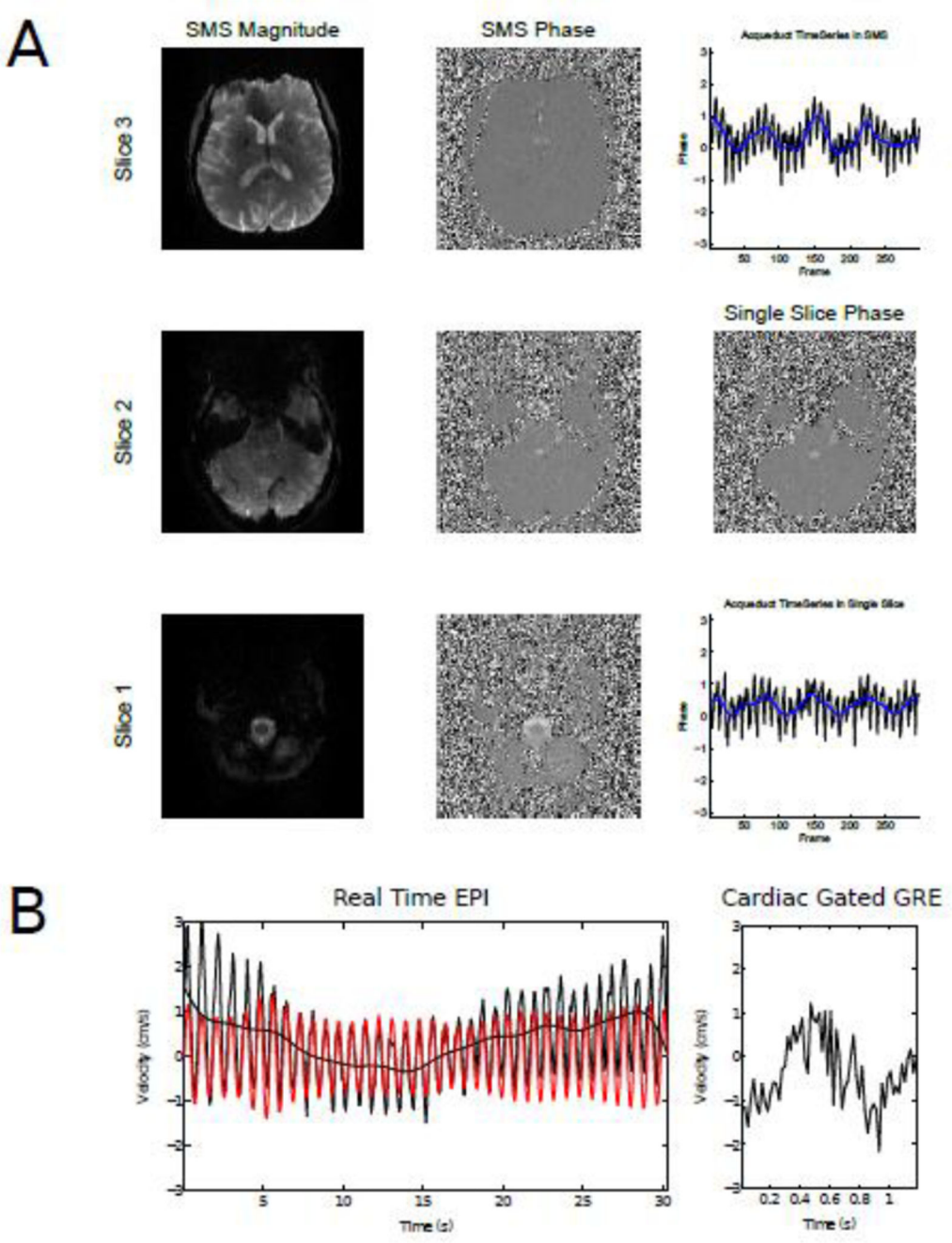

Figure 2.

Comparison of SMS and single slice velocity encoded images. Magnitude and phase contrast images from 3 slices from an SMS acquisition are shown, with the equivalent phase image from a single slice acquisition. ROI timeseries from the aqueduct are also shown for the SMS and single-slice acquisitions. (Bottom) CSF velocities measured in the aqueduct with SMS-EPI (left) and GRE phase contrast imaging (right). The red plot shows a band-passed timeseries, corresponding to cardiac modulations.

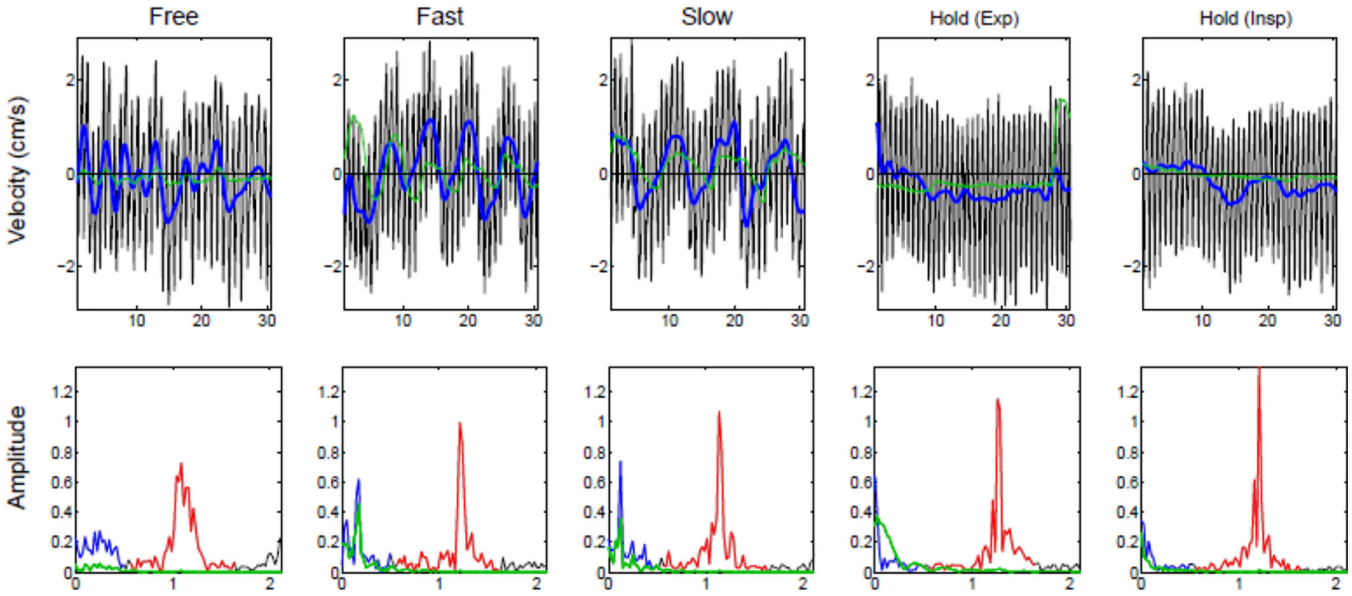

Figure 3.

CSF velocities in the aqueduct of a single subject during five different breathing schemes: free breathing, fast breathing, slow breathing and breath-hold after expiration and inspiration. The velocity curve from the aqueduct is shown in the top row: the low-passed data (< 0.5 Hz) is shown (thick blue line), and measurements simultaneously acquired with a respiratory belt (green) are shown. The Fourier transform of the data is shown in the bottom row, with the (red) respiratory (< 0.5 Hz) and (blue) cardiac (~ 1.1 Hz) frequency bands highlighted, respectively, and data from the respiratory belt (green) is plotted.

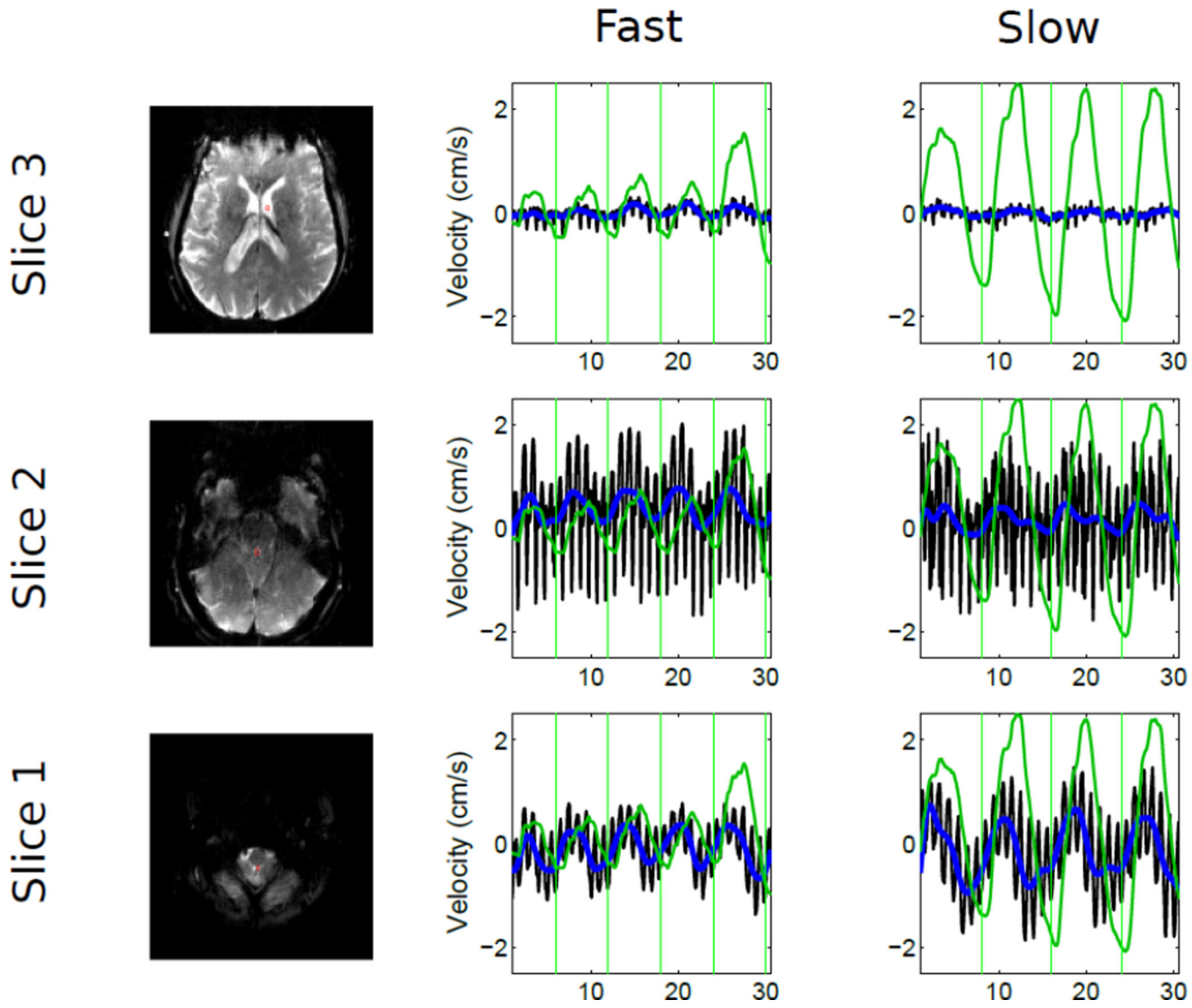

Figure 4.

Velocities measured simultaneously in 2 slices across 7 subjects during cued breathing at two different frequencies. Plotting of the timeseries data has the same color convention as Figure 3. Vertical green lines indicate the start of externally cued inspiration.

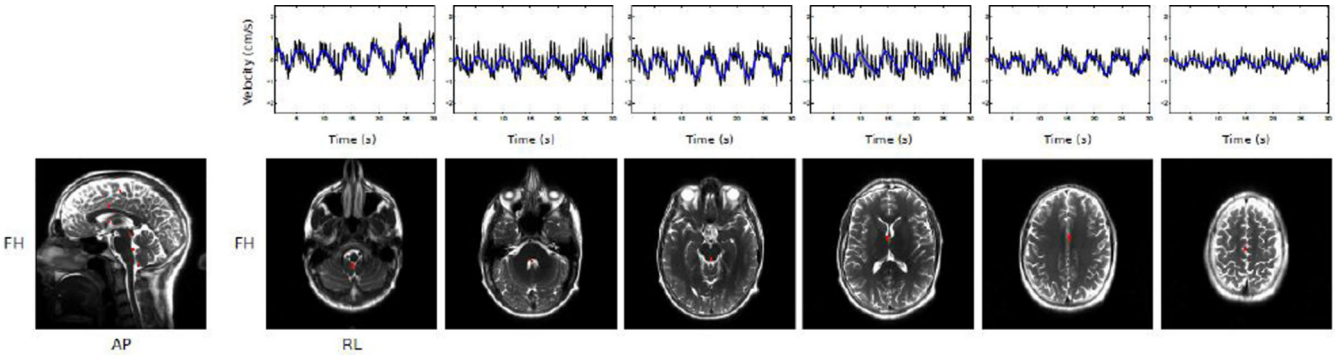

Figure 5.

Velocities measured in 6 simultaneously acquired slices. Timeseries data is plotted with the same conventions as Figure 2 (raw data in black, low-passed data in blue).

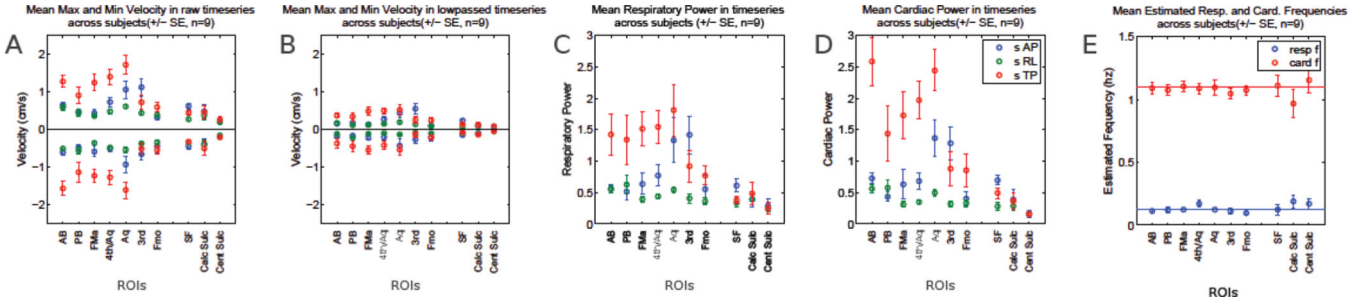

Figure 6.

Data from whole brain 24 slice data, showing different measures across 9 subjects. A) Minimum and maximum velocities in the raw data velocity data. SI = red, AP = blue, right-left (RL) = green. B) Minimum and maximum velocities for each ROI in each direction in low-pass (< 0.5 Hz) filtered data. Same plotting convention as A. C) Mean respiratory power (total amplitudes for frequencies < 0.5 Hz). D) Mean cardiac power (frequencies between 0.6 and 1.5 Hz). Same convention as C. E) Peak frequencies for each ROI in the respiratory (blue) and cardiac (red) frequency ranges for the SI direction. ROI abbreviations: Posterior Basal Cistern (PB), Anterior Basal (AB), Foramen of Magendie (FMa), 4th Ventricle/ Aqueduct (4th/Aq), Aqueduct (Aq), 3rd Ventricle (3rd), Foramen of Monroe (FMo), Sylvain Fissure (SF), Calcarine Sulcus (Calc Sulc), Central Sulcus (Cent Culc).